Femtosecond Pump−Probe Spectroscopy of Trinuclear Transition Metal Mixed-Valence Complexes

David F. Watson, Howe Siang Tan, Elmar Schreiber, Carolyn J. Mordas, and Andrew B. Bocarsly*

Department of Chemistry and Center for Ultrafast Laser Applications, Frick Laboratory, Princeton University, Princeton, New Jersey 08544

Received: August 5, 2003; In Final Form: December 31, 2003

The dynamics of relaxation following photoinduced metal-to-metal charge-transfer (MMCT) processes of the trinuclear mixed-valence complexes $[(NC)_5Ru^{II}-CN-Pt^{IV}(NH_3)_4-NC-Ru^{II}(CN)_5]^{4-}$ and $[(NC)_5Fe^{II}-CN-Pt^{IV}(NH_3)_4-NC-Fe^{II}(CN)_5]^{4-}$ were investigated with femtosecond pump−probe spectroscopy. Relaxation dynamics following photoinduced M(II) → Pt(IV) MMCT varied with solvent and the identity of the M(II) centers. The back-electron-transfer (BET) time scale of $[(NC)_5Ru^{II}-CN-Pt^{IV}(NH_3)_4-NC-Ru^{II}(CN)_5]^{4-}$ ranged from 476 ± 23 fs in water to 1110 ± 288 fs in a water/DMSO mixture with mole fraction DMSO of 0.1. The time scale of vibrational relaxation in the ground state ranged from 1.5 to 2.7 ps. Electron-transfer and ground-state vibrational relaxation dynamics of $[(NC)_5Fe^{II}-CN-Pt^{IV}(NH_3)_4-NC-Fe^{II}(CN)_5]^{4-}$ were convolved, with relaxation to ground and product electronic states occurring within 3.5 ps. The electron-transfer dynamics of both complexes are significantly slower than the solvation dynamics of water or DMSO. The solvent dependence of the BET time scale of $[(NC)_5Ru^{II}-CN-Pt^{IV}(NH_3)_4-NC-Ru^{II}(CN)_5]^{4-}$ is attributed to solvent-induced movement of the ground-state potential energy surface and the resulting changes in the driving force for BET. These effects enable systematic control over both the quantum yield of photodissociation and the dynamics of relaxation following photoinduced MMCT.

Introduction

Transition metal mixed-valence complexes have played an important role in the development and experimental verification of electron-transfer theory.[1−6] In addition, the photoinduced electron-transfer processes occurring in mixed-valence complexes have potential for application in energy conversion and photocatalysis. Our laboratory has extensively characterized the trinuclear mixed-valence complexes $[(NC)_5Ru^{II}-CN-Pt^{IV}(NH_3)_4-NC-Ru^{II}(CN)_5]^{4-}$ and $[(NC)_5Fe^{II}-CN-Pt^{IV}(NH_3)_4-NC-Fe^{II}(CN)_5]^{4-}$ (herein referred to as Ru(II)−Pt(IV)−Ru(II) and Fe(II)−Pt(IV)−Fe(II), respectively).[7−10] These complexes undergo photoinduced M(II) → Pt(IV) metal-to-metal charge-transfer (MMCT), generating the one-electron-transfer intermediate M(III)−Pt(III)−M(II). Decay of the intermediate occurs either through back electron transfer to yield the M(II)−Pt(IV)−M(II) starting material or through thermal MMCT from the remaining M(II) center to the Pt(III) center to yield 2 equiv of $M^{III}(CN)_6^{3-}$ and 1 equiv of $Pt^{II}(NH_3)_4^{2+}$. The photodissociation quantum yields of Ru(II)−Pt(IV)−Ru(II) and Fe(II)−Pt(IV)−Fe(II) are 0.001 and 0.02, respectively.[7,11] The two-electron-transfer photodissociative chemistry of the M(II)−Pt(IV)−M(II) complexes is unique among mixed-valence complexes reported to date, rendering the trinuclear complexes as interesting models of photoinduced multiple-electron-transfer systems.

The electronic properties of the M(II)−Pt(IV)−M(II) complexes are accurately characterized by a three parabola free energy diagram.[9,10,12−14] Three potential energy surfaces are required to describe the available electronic configurations: M(II)−Pt(IV)−M(II), M(III)−Pt(III)−M(II), and M(III)/Pt(II)/M(III). The M(II) → Pt(IV) MMCT energy depends linearly on the $M^{III/II}$ reduction potential ($E_{1/2}(M^{III/II})$).[9,10] Shifts of $E_{1/2}(M^{III/II})$ correspond to shifts of the M(II)−Pt(IV)−M(II) (ground electronic state) potential energy surface. Our lab has studied the MMCT processes of Fe(II)−Pt(IV)−Fe(II) in water/DMSO mixed solvent systems.[9,10,15] A linear dependence of $E_{1/2}(Fe^{III/II})$ on mole fraction DMSO (χ_{DMSO}) was observed, with $E_{1/2}(Fe^{III/II})$ shifting negatively with increasing χ_{DMSO}. The Fe(II) → Pt(IV) MMCT energy decreased linearly with increasing χ_{DMSO}, whereas the quantum yield of the two-electron-transfer photodissociative process increased exponentially. These changes are consistent with a linear dependence of the Fe(II)−Pt(IV)−Fe(II) potential energy on χ_{DMSO}. Thus, the solvent dependence of $E_{1/2}(M^{III/II})$ allows for control over the activation barrier and driving force of forward- and back-electron-transfer processes following photoinduced M(II) → Pt(IV) MMCT.

This manuscript describes femtosecond pump−probe experiments on Ru(II)−Pt(IV)−Ru(II) and Fe(II)−Pt(IV)−Fe(II). One-color and two-color pump−probe data are presented. We have studied the effects of solvent-induced movement of potential energy surfaces on the relaxation dynamics following photoinduced MMCT and the role of a photoinduced charge transfer rapidly followed by a thermal electron transfer as a model of photoinduced multielectron-transfer processes.

Experimental Section

Materials and Basic Instrumentation. $K_4Ru(CN)_6 \cdot 3H_2O$ was purchased from Pressure Chemical Co. $K_3Fe(CN)_6$ was purchased from Fisher Scientific. $Ce(SO_4)_2$ and $Pt(NH_3)_4(NO_3)_2$ were purchased from Aldrich. Reagents were used without further purification. Amberlite IR-120 sodium exchange column resin was purchased from Aldrich. Bio-Gel P-2 size exclusion column resin was purchased from Bio-Rad. UV/visible absorp-

10.1021/jp0363038 CCC: $27.50
Published on Web 03/23/2004

tion spectra were obtained with a Hewlett-Packard HP8453 diode array spectrophotometer.

Synthesis. $Na_4[(NC)_5Ru^{II}-CN-Pt^{IV}(NH_3)_4-NC-Ru^{II}(CN)_5]$ was synthesized by adaptation of the method of Pfennig and Bocarsly.[9] An aqueous solution of $K_4Ru(CN)_6 \cdot 3H_2O$ (3.90 mmol, 46 mL) was oxidized to $Ru^{III}(CN)_6^{3-}$ by addition of aqueous $Ce(SO_4)_2$. The reaction mixture was filtered by gravity and then run through an Amberlite IR-120 sodium exchange column charged with 1.0 M NaCl solution to remove Ce^{4+} and Ce^{3+}. To the $Ru^{III}(CN)_6^{3-}$ solution was added aqueous $Pt(NH_3)_4(NO_3)_2$ (3.53 mmol, 46 mL). The reaction mixture was stirred at room temperature under subdued lighting for 90 min, then concentrated and run through an Amberlite IR-120 sodium exchange column charged with 1.0 M NaCl solution to remove excess $Pt(NH_3)_4^{2+}$ and then run through a Bio-Gel P-2 size exclusion column. The product was collected in fractions, which were analyzed by UV/visible absorption spectroscopy. Pure fractions were combined and air-dried, yielding the desired product.

$Na_4[(NC)_5Fe^{II}-CN-Pt^{IV}(NH_3)_4-NC-Fe^{II}(CN)_5]$ was synthesized by adaptation of the method of Zhou et al.[7] Aqueous solutions of $K_3Fe(CN)_6$ (1.20 mmol, 5.0 mL) and $Pt(NH_3)_4(NO_3)_2$ (0.520 mmol, 5.0 mL) were combined at room temperature under subdued lighting. The resulting deep red solution was run through an Amberlite IR-120 sodium exchange column charged with 1.0 M NaCl solution, then through a Bio-Gel P-2 size exclusion column. The product was collected in fractions, which were analyzed for $Fe(CN)_6^{3-}$ impurity by cyclic voltammetry. Pure fractions were combined and air-dried, yielding the desired product.

Pump−Probe Spectroscopy. Pulses at 400 nm were generated by frequency doubling the 800 nm output of a regeneratively amplified Ti:sapphire oscillator (Spectra-Physics). In one-color pump−probe experiments, the 400 nm beam was attenuated and split into pump (400 nm, 10 μJ, ~150 fs, 1 kHz) and probe (400 nm, <10 nJ, ~150 fs, 1 kHz) beams. The probe beam was aligned through a high-precision translation stage with 0.2 fs resolution (Physik Instrumente C844−40), acting as a variable path length delay line. The pump and probe beams were focused (f = 100 mm) into the flowing sample (0.25 mL/s in a 1 cm cuvette) at an angle of 6°. The pump beam was chopped (90−150 Hz), and the oscillatory component of the probe signal was measured with lock-in technique. In two-color pump−probe experiments, pump pulses (400 nm, 6 μJ, 100 fs, 1 kHz) were generated as described above. Probe pulses (532 nm, <1 nJ, 25 fs, 1 kHz) were generated using a noncollinear optical parametric amplification (NOPA) process, following the method of Riedle and co-workers.[16−19] A portion of the 800 nm regenerative amplifier output was split into two components. The weak component (~10 μJ) was used to generate a white light continuum (WLC) in a 2 mm sapphire plate. The strong component (680 μJ) was frequency doubled to 400 nm (190 μJ). The WLC was focused into a 2 mm β-BBO crystal, and the 400 nm pulses (attenuated to ~90 μJ) were focused to a point 20 mm in front of the β-BBO crystal. NOPA produced pulses from 630 nm (13 μJ) to 515 nm (9 μJ) with ~25 fs pulse width. Tunability of the amplified wavelength and minimization of pulse width was achieved by varying the angle and temporal delay between the 400 nm pump and the WLC seed, and by rotating the β-BBO crystal. Two-color pump−probe experiments employed the setup and detection mechanisms described above. For most one-color and two-color experiments, pump and probe polarizations were parallel. For some experiments, the probe polarization was rotated 90° with a half-wave plate.

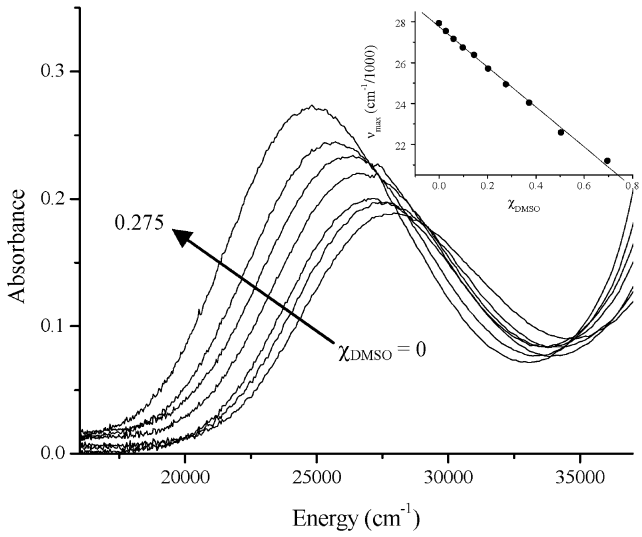

Figure 1. UV/visible absorption spectra of 0.1 mM Ru(II)−Pt(IV)−Ru(II) in water/DMSO solvent mixtures with χ_{DMSO} = 0, 0.0275, 0.06, 0.1, 0.15, 0.2025, 0.275. Cuvette path length = 1.0 cm. Inset: plot of MMCT absorption maximum (ν_{max}) vs χ_{DMSO} and fit to a straight line (R^2 = 0.996).

Results

Solvent-Dependent MMCT Energy of Ru(II)−Pt(IV)−Ru(II). Ground-state UV/visible absorption spectra of Ru(II)−Pt(IV)−Ru(II) were obtained in water/DMSO mixtures of varying composition (Figure 1). The energy of the MMCT band maximum decreases linearly with increasing χ_{DMSO} (Figure 1 inset), whereas the absorption bandwidth remains the same. The linear red shift of the MMCT band with χ_{DMSO} is consistent with a linear shift of the Ru(II)−Pt(IV)−Ru(II) potential energy surface to higher energy, as previously observed with Fe(II)−Pt(IV)−Fe(II).[10]

One-Color Pump−Probe Data. One-color pump−probe data (400 nm pump, 400 nm probe) were acquired for Ru(II)−Pt(IV)−Ru(II) in water, Ru(II)−Pt(IV)−Ru(II) in water/DMSO solvent mixtures, and Fe(II)−Pt(IV)−Fe(II) in water. Representative data are shown in Figure 2. The data are plotted as the normalized negative absorbance change ($-\Delta A$) vs time (t). Positive values on the vertical axis correspond to a decreased absorbance or bleach, whereas negative values on the vertical axis correspond to an increased absorbance. The system response (Figure 2a) is well approximated by a Gaussian intensity profile and is assigned as a cross-phase modulation-induced artifact.[20−24]

In the data for Ru(II)−Pt(IV)−Ru(II) in water (Figure 2b), two signals are present at very short delay times: the cross-phase modulation-induced artifact and an absorptive signal. The absorptive signal is tentatively assigned to an excited-state absorption process originating from the vibrationally excited one-electron charge-transfer excited state, Ru(III)−Pt(III)−Ru(II)*. It is not unreasonable that the excited state undergoes absorption at 400 nm, because Ru(II)−Pt(IV)−Ru(II) absorbs strongly at 200 nm. Sequential 400 nm absorptions are energetically equivalent to a single 200 nm absorption. The absorptive signal is more clearly visible in data with perpendicular pump and probe polarizations, as discussed below.

Within 600 fs, the excited-state absorption decays to a bleach. The transition from an absorptive signal to a bleach signifies that the decrease of absorbance from depletion of the ground-state outweighs the increase of absorbance from the excited-state absorption process. Vibrational relaxation within the Ru(III)−Pt(III)−Ru(II)* electronic excited state necessarily

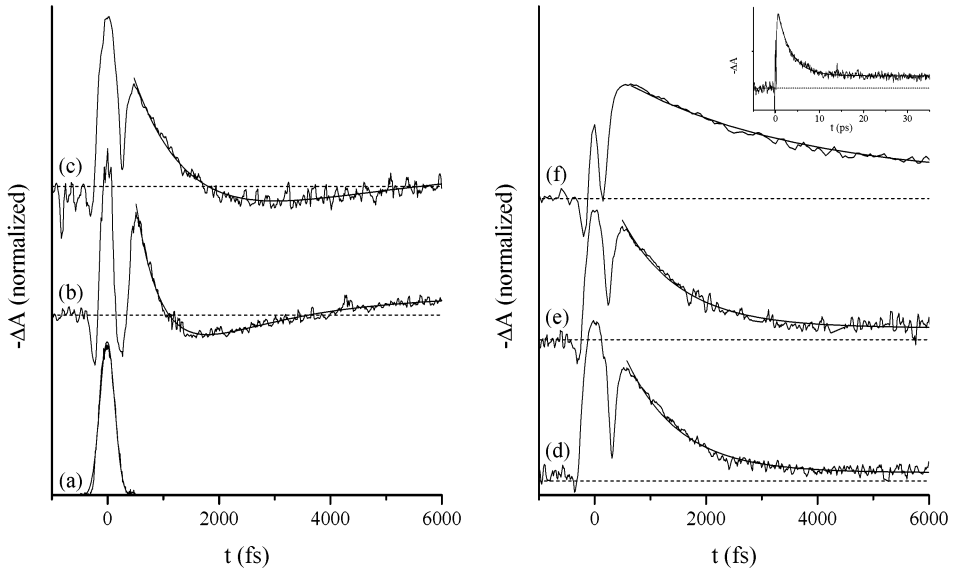

Figure 2. One-color pump−probe data (400 nm) with parallel pump and probe polarizations: (a) cross-phase modulation-induced artifactual signal with water in sample cuvette; (b) Ru(II)−Pt(IV)−Ru(II), $\chi_{DMSO} = 0$; (c) Ru(II)−Pt(IV)−Ru(II), $\chi_{DMSO} = 0.1$; (d) Ru(II)−Pt(IV)−Ru(II), $\chi_{DMSO} = 0.175$; (e) Ru(II)−Pt(IV)−Ru(II), $\chi_{DMSO} = 0.2$; (f) Fe(II)−Pt(IV)−Fe(II), $\chi_{DMSO} = 0$ (inset shows same data on longer time scale). In each plot, the dashed line corresponds to $-\Delta A = 0$. Superimposed on the system response data is a Gaussian fit. Superimposed on the M(II)−Pt(IV)−M(II) data are fits to eq 1 (b, c) or 2 (d, e, f).

leads to a significant blue shift of the excited-state absorption, as the vertical transition to a higher lying electronic state occurs at higher energy. A strong blue shift of the excited-state absorption is consistent with the disappearance of the absorptive signal at 400 nm. We therefore propose that the time scale for evolution of the signal to the bleach maximum corresponds to the time scale of vibrational relaxation in the electronic excited state. Accordingly, we assign the bleach maximum to the vibrationally relaxed, one-electron charge-transfer intermediate Ru(III)−Pt(III)−Ru(II).

The bleach corresponding to Ru(III)−Pt(III)−Ru(II) decays to an absorptive signal. The evolution of the bleach to the absorptive signal is consistent with the population of vibrationally excited states in the ground electronic state following back electron transfer. The Ru(II) → Pt(IV) MMCT transition from vibrationally excited states in the ground electronic state must be red-shifted relative to the MMCT transition from lower-lying vibrational states, due to the decreased energy of vertical excitation. Because the 400 nm probe pulse is slightly to the red of the ground-state MMCT band maximum of aqueous Ru(II)−Pt(IV)−Ru(II), a dynamic red shift of the MMCT band should cause an increase of absorbance at 400 nm, consistent with the observed absorptive signal. We therefore correlate the time scale for evolution of the data from the bleach to the absorption with the time scale of electron transfer from the vibrationally relaxed one-electron-transfer intermediate, Ru(III)−Pt(III)−Ru(II), to vibrationally excited levels in the ground electronic state, Ru(II)−Pt(IV)−Ru(II). We note that the decay of Ru(III)−Pt(III)−Ru(II) can occur either through back electron transfer (BET) to yield Ru(II)−Pt(IV)−Ru(II) or through "forward electron transfer" (FET) to yield the two-electron-transfer product Ru(III)/Pt(II)/Ru(III). On the basis of the two-electron-transfer quantum yield of 0.001, the decay of the bleach must correspond primarily to BET. Separation of BET and FET dynamics will be discussed below.

Our assignment of the absorptive signal at ∼1500 fs to MMCT from the vibrationally excited ground electronic state is not without precedence. Barbara and co-workers have reported similar absorptive signals following decay of the excited-state bleach in pump−probe experiments on the organic mixed-valence complexes betaine-30 and *tert*-butylbetaine, and the dinuclear transition metal mixed-valence complex $[(H_3N)_5Ru^{III}$-NC−$Ru^{II}(CN)_5]^-$.[25−31] The absorptive signals were only observed with probe wavelengths to the red of the ground-state absorption maxima, consistent with our findings.[27−31] Barbara and co-workers assigned the absorptive signals to red-shifted charge-transfer bands from vibrationally excited levels of the ground electronic states.[28−31]

For Ru(II)−Pt(IV)−Ru(II) in water, the absorptive signal decays to a long-lived bleach (τ > 100 ps), which is assigned to depletion of the Ru(II)−Pt(IV)−Ru(II) ground state through formation of the two-electron-transfer product Ru(III)/Pt(II)/Ru(III) by FET. This assignment is justified by the absence of a long-lived bleach for the dinuclear complex $[(H_3N)_5Ru^{III}$-NC−$Ru^{II}(CN)_5]^-$. The absorptive signal of $[(H_3N)_5Ru^{III}$-NC−$Ru^{II}(CN)_5]^-$ decays to the baseline absorbance within 10 ps, completing the dynamics following photoinduced charge transfer.[27−30] The main difference between the trinuclear and dinuclear complexes is the existence of the third potential energy surface in the trinuclear complex, and therefore the second available decay pathway from the one-electron-transfer intermediate, Ru(III)−Pt(III)−Ru(II). The M(II)−Pt(IV)−M(II) complexes are unique among mixed-valence complexes in this regard. In the data for Ru(II)−Pt(IV)−Ru(II), the time scale for the evolution of the absorptive signal to the long-lived bleach corresponds to the time scales of vibrational relaxation in the ground and product electronic states.

The one-color pump−probe data for Ru(II)−Pt(IV)−Ru(II) in water/DMSO mixtures with $\chi_{DMSO} \leq 0.1$ (Figure 2c) exhibit similar features to the data for aqueous Ru(II)−Pt(IV)−Ru(II). The one-color data for Ru(II)−Pt(IV)−Ru(II) in water/DMSO mixtures with $\chi_{DMSO} > 0.1$ (Figure 2d,e) and for Fe(II)−Pt(IV)−Fe(II) in water (Figure 2f) exhibit no absorptive signal following decay from the one-electron-transfer intermediate. In the Ru(II)−Pt(IV)−Ru(II) mixed-solvent case, at sufficiently high χ_{DMSO} the ground-state MMCT absorption maximum approaches 400 nm. Thus, a dynamic red shift of the MMCT band upon population of vibrationally excited levels in the ground electronic state following BET must cause a negligible increase in the absorbance at 400 nm. For aqueous Fe(II)−Pt(IV)−Fe(II) the

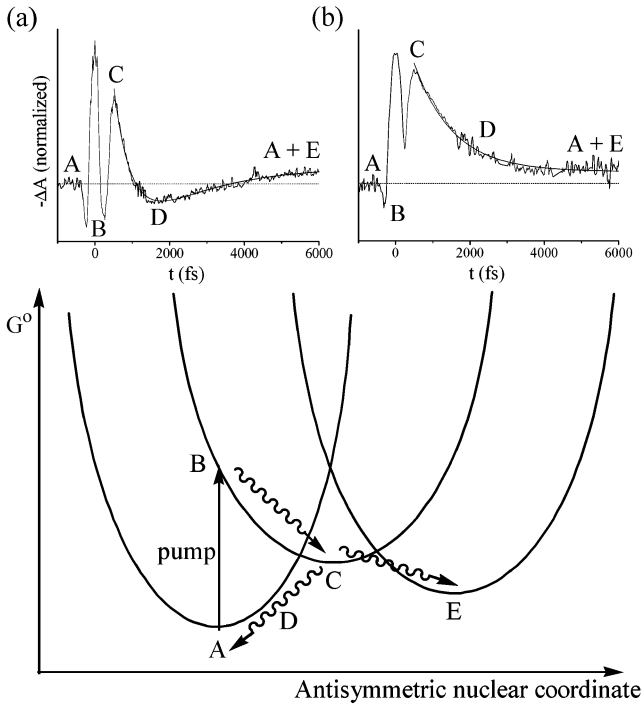

Figure 3. Interpretation of one-color pump−probe data for Ru(II)−Pt(IV)−Ru(II) in water (a) and in a water/DMSO mixture with $\chi_{DMSO} = 0.2$ (b). At $t<0$, the Ru(II)−Pt(IV)−Ru(II) ground state (A) is populated. Pump absorption creates population in the vibrationally excited electronic excited state, Ru(II)−Pt(III)−Ru(III)* (B), from which an excited-state absorption occurs (convolved with the artifactual signal). The excited state decays to the one-electron-transfer state, Ru(II)−Pt(III)−Ru(III) (C), corresponding to a bleach. Decay through BET or FET yields Ru(II)−Pt(IV)−Ru(II) (A) or Ru(III)/Pt(II)/Ru(III) (E). Vibrational relaxation in the ground electronic state (D) corresponds to either an absorptive signal (as in a) or a bleach (as in b), depending on the relative energies of the ground-state MMCT maximum and the probe beam.

ground-state absorption maximum is to the red of the probe wavelength, so the dynamic red shift of the MMCT band following BET must cause a decrease in the absorbance at 400 nm. Therefore, in both cases the decay of the excited-state bleach directly to a long-lived bleach is consistent with our expectations based on the relative wavelengths of the probe and the ground-state MMCT maxima. In these data, the time scale for decay of the excited-state bleach represents a convolution of electron-transfer dynamics with vibrational relaxation dynamics. It has been well documented that the appearance of an absorption or a bleach following the initial excited-state bleach depends on the relative energies of the ground-state absorption maximum and the probe beam.[25−31]

The data for aqueous Fe(II)−Pt(IV)−Fe(II) evolves to a long-lived bleach ($\tau > 100$ ps) corresponding to formation of the two-electron charge-transfer product (Figure 2f, inset). The magnitude of the long-lived bleach in the data for Fe(II)−Pt(IV)−Fe(II) is significantly greater than the magnitude of the corresponding bleach for Ru(II)−Pt(IV)−Ru(II). This trend is consistent with the greater photodissociation quantum yield of Fe(II)−Pt(IV)−Fe(II). Our interpretation of the one-color pump−probe data for Ru(II)−Pt(IV)−Ru(II) and Fe(II)−Pt(IV)−Fe(II) is summarized in Figure 3.

Polarization Dependence of One-Color Pump−Probe Signal. One-color pump−probe data with perpendicular pump and probe polarizations were acquired for Ru(II)−Pt(IV)−Ru(II) and Fe(II)−Pt(IV)−Fe(II) in water (Figure 4). The system response signal at the zero of time is greatly diminished, consistent with its assignment as a cross-phase modulation-induced artifact. In the data for Ru(II)−Pt(IV)−Ru(II), a strong absorptive signal is observed at short delay times. This excited-state absorption was largely obscured by the artifactual signal in the data with parallel pump and probe polarizations. The absorptive signal decays to the bleach corresponding to the Ru(III)−Pt(III)−Ru(II)* excited state. The bleach is diminished, due to the orientation of the transition dipole along the *z*-axis of the molecule. In the data for Fe(II)−Pt(IV)−Fe(II), the decay of the absorptive signal to the bleach, corresponding to vibrational relaxation in the Fe(III)−Pt(III)−Fe(II)* excited state, was fit to single-exponential kinetics with a rise time of 141 ± 7 fs. Data at subsequent delay times exhibited minimal polarization dependence.

Two-Color Pump−Probe Data. Two-color pump−probe data (400 nm pump, 532 nm probe) were acquired for Ru(II)−Pt(IV)−Ru(II) in water, Ru(II)−Pt(IV)−Ru(II) in water/DMSO mixtures, and Fe(II)−Pt(IV)−Fe(II) in water. Representative data are shown in Figure 5. In each data set, a cross-phase modulation-induced artifact is present at the zero of time. In all Ru(II)−Pt(IV)−Ru(II) data (Figure 5b−e), a bleach arises directly from the artifact, indicating that excited-state absorption is insignificant at 532 nm. In the Fe(II)−Pt(IV)−Fe(II) data (Figure 5f), the rise time of the bleach is slower, suggesting

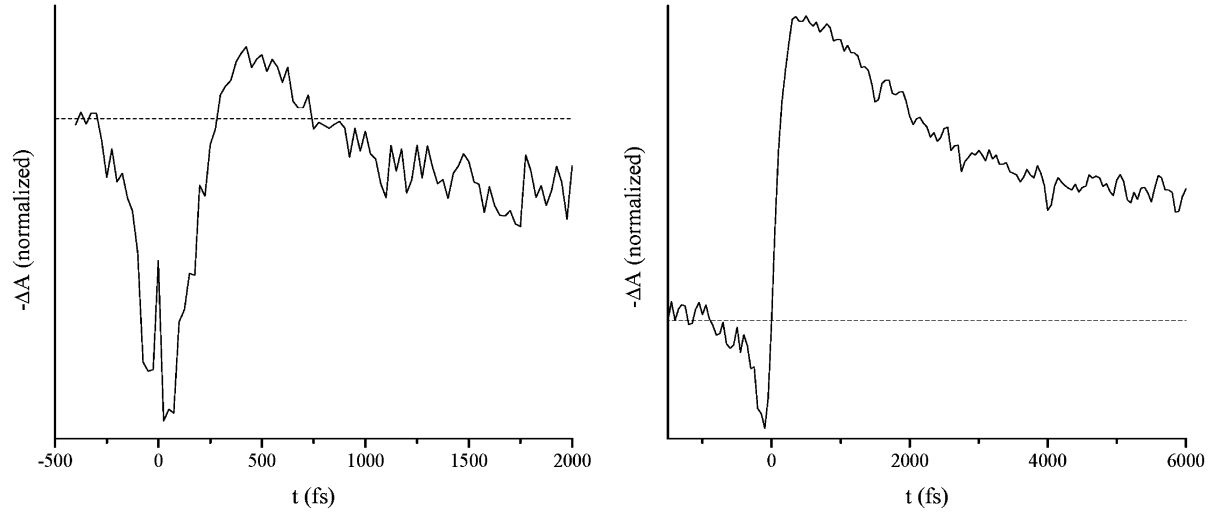

Figure 4. One-color pump−probe data (400 nm) with perpendicular pump and probe polarizations: (a) Ru(II)−Pt(IV)−Ru(II); (b) Fe(II)−Pt(IV)−Fe(II). In each plot, the dashed line corresponds to $-\Delta A = 0$.

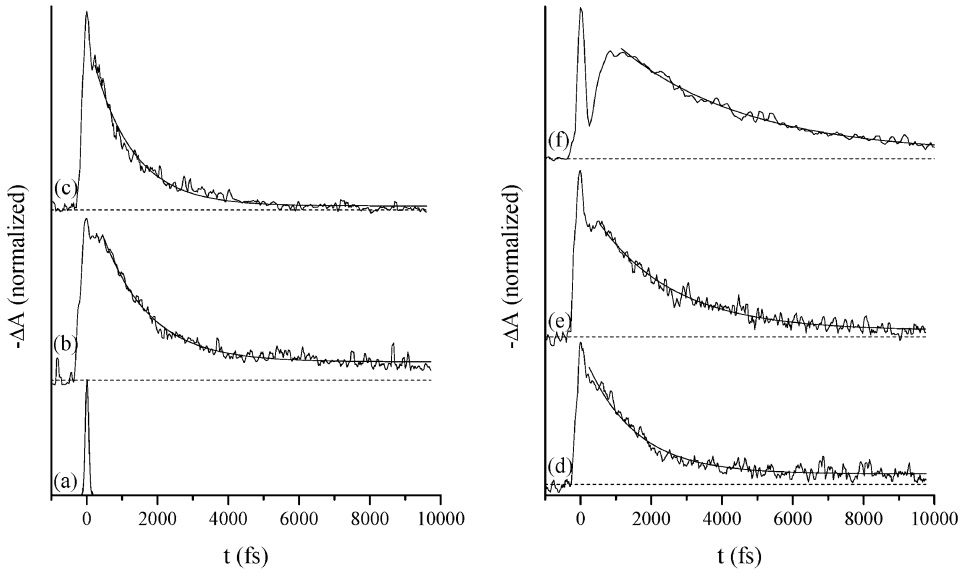

Figure 5. Two-color pump−probe data (400 nm pump, 532 nm probe) with parallel pump and probe polarizations: (a) cross-phase modulation-induced artifactual signal with water in sample cuvette; (b) Ru(II)−Pt(IV)−Ru(II), $\chi_{DMSO} = 0$; (c) Ru(II)−Pt(IV)−Ru(II), $\chi_{DMSO} = 0.025$; (d) Ru(II)−Pt(IV)−Ru(II), $\chi_{DMSO} = 0.05$; (e) Ru(II)−Pt(IV)−Ru(II), $\chi_{DMSO} = 0.175$; (f) Fe(II)−Pt(IV)−Fe(II), $\chi_{DMSO} = 0$. In each plot, the dashed line corresponds to $-\Delta A = 0$. Superimposed on the artifactual signal is a Gaussian fit. Superimposed on the M(II)−Pt(IV)−M(II) data are fits to eq 2.

that excited-state absorption at 532 nm occurs at very short delay times. As in the one-color data, the bleach is assigned to the decrease of ground-state MMCT absorption due to population of the vibrationally relaxed one-electron-transfer intermediate M(III)−Pt(III)−M(II). For all samples this bleach decays directly to a long-lived bleach, which is assigned to product formation. Although the probe beam is to the red of the ground-state MMCT maxima of all samples, no absorptive signal corresponding to MMCT from vibrationally excited states in the ground electronic state is observed. We interpret the lack of absorptive signal to narrowing of the MMCT absorption band from vibrationally excited levels in the ground electronic state. Because of the displacement of the vibrationally excited ground-state wave packet along the nuclear coordinate axis, vertical excitation should populate a decreased number of vibrational states in the excited electronic state. The lack of an absorptive signal in the two-color data suggests that the decrease of absorbance at 532 nm from narrowing of the MMCT band is greater than the increase of absorbance at 532 nm from red-shifting of the MMCT band. The MMCT band should blue shift and broaden upon vibrational relaxation in the ground state, giving rise to increased absorbance at 532 nm. Thus, the observed bleach decay contains components from both electron-transfer dynamics and vibrational relaxation dynamics.

Discussion

Extracting electron-transfer rate constants from pump−probe data can be nontrivial, because in certain cases vibrational relaxation dynamics obscure electron-transfer dynamics. However, electron-transfer rate constants are readily determined from the one-color data for Ru(II)−Pt(IV)−Ru(II) with $\chi_{DMSO} \leq 0.1$. The presence of the absorptive signal following the excited-state bleach in these data enables straightforward deconvolution of electron-transfer dynamics and ground-state vibrational relaxation dynamics. The one-electron-transfer intermediate Ru(III)−Pt(III)−Ru(II) decays through the parallel pathways of BET or FET (Figure 3). Therefore, a branching first-order kinetic model should accurately fit the decay of the observed bleach. In this model, the formation of Ru(II)−Pt(IV)−Ru(II) and Ru(III)/Pt(II)/Ru(III) occurs with the same rate, with a rate constant $k_{ET} = k_{BET} + k_{FET}$. Vibrational relaxation in the ground electronic state should occur with first-order kinetics. The one-color data for Ru(II)−Pt(IV)−Ru(II) with $\chi_{DMSO} \leq 0.1$ were accurately modeled by the biexponential decay function

$$\Delta A(t) = \Delta A_0 + C_1 e^{-k_{ET}t} + C_2 e^{-k_{VR}t} \quad (1)$$

where $\Delta A(t)$ is the time-dependent absorbance difference, ΔA_0 is the absorbance difference of the long-lived bleach, C_1 and C_2 are preexponential weighting factors, t is the delay time, k_{ET} is the electron-transfer rate constant ($k_{ET} = k_{BET} + k_{FET}$), and k_{VR} is the vibrational relaxation rate constant. The one-color data for Fe(II)−Pt(IV)−Fe(II) and Ru(II)−Pt(IV)−Ru(II) with $\chi_{DMSO} > 0.1$ and all two-color data obeyed pseudo-first-order kinetics. These data were accurately modeled by the single-exponential function

$$\Delta A(t) = \Delta A_0 + C_1 e^{-k_{obs}t} \quad (2)$$

where k_{obs} must correspond to a convolution of k_{BET}, k_{FET}, and k_{VR}. Kinetic modeling results are summarized in Table 1.

The dynamics of relaxation following photoinduced MMCT are solvent dependent. The one-color data for Ru(II)−Pt(IV)−Ru(II) with $\chi_{DMSO} \leq 0.1$ are the most useful in interpreting this effect, as these data allowed for deconvolution of k_{ET} and k_{VR}. In the following discussion of solvent-dependent relaxation dynamics, we focus primarily on these data. Inspection of Table 1 reveals that k_{ET} decreases with increasing χ_{DMSO}, whereas k_{VR} is relatively independent of solvent. The decrease of k_{ET} with increasing χ_{DMSO} could arise from either changes in the dynamics of solvent reorganization or solvent-induced shifts of the Ru(II)−Pt(IV)−Ru(II) ground-state potential energy surface.

The solvent response to intramolecular electron transfer in the solute generally consists of multiple components, corresponding to inertial (uncoupled translational and rotational) motion of individual solvent molecules on time scales ranging from tens to hundreds of femtoseconds, and coupled diffusional motion on time scales ranging from several picoseconds to

TABLE 1: Kinetic Modeling Parameters for Pump−Probe Data of Ru(II)−Pt(IV)−Ru(II) and Fe(II)−Pt(IV)−Fe(II)[a]

(a) One-Color Data Modeled by Eq 1
$\lambda_{pump} = 400$ nm, $\lambda_{probe} = 400$ nm

sample	χ_{DMSO}	τ_{ET} (fs)[b]	τ_{VR} (fs)[b]	C_1[c]	C_2[c]
Ru(II)−Pt(IV)−Ru(II)	0	476 ± 23	1890 ± 215	−0.80	0.20
	0.0125	796 ± 179	1395 ± 410	−0.61	0.39
	0.025	836 ± 142	1650 ± 482	−0.65	0.35
	0.0375	861 ± 275	1465 ± 737	−0.62	0.38
	0.05	988 ± 196	2750 ± 1328	−0.63	0.37
	0.1	1110 ± 288	2720 ± 2130	−0.67	0.33

(b) One-Color Data Modeled by Eq 2
$\lambda_{pump} = 400$ nm, $\lambda_{probe} = 400$ nm

sample	χ_{DMSO}	τ_{obs} (fs)[b]
Ru(II)−Pt(IV)−Ru(II)	0.175	956 ± 16
	0.2	1047 ± 23
	0.225	1335 ± 39
Fe(II)−Pt(IV)−Fe(II)	0	3160 ± 46

(c) Two-Color Data Modeled by Eq 2
$\lambda_{pump} = 400$ nm, $\lambda_{probe} = 532$ nm

sample	χ_{DMSO}	τ_{obs} (fs)[b]
Ru(II)−Pt(IV)−Ru(II)	0	980 ± 19
	0.025	1138 ± 21
	0.05	1397 ± 35
	0.175	2148 ± 53
Fe(II)−Pt(IV)−Fe(II)	0	3590 ± 87

[a] Data that exhibit the absorptive signal following bleach decay were fit to the biexponential function (eq 1). Data that exhibit pseudo-first-order bleach decay kinetics were fit to the single-exponential function (eq 2). [b] $\tau_{ET} = 1/k_{ET}$, $\tau_{VR} = 1/k_{VR}$, $\tau_{obs} = 1/k_{obs}$. [c] Amplitudes are normalized such that $|C_1| + |C_2| = 1$.

hundreds of picoseconds.[32−35] The solvation dynamics of water consist of three components, with time scales of 50, 126, and 880 fs. The relative contributions of these components to the overall solvent response are approximately 50%, 20%, and 35%.[33] The fast components have been attributed to inertial solvation, whereas the slowest component has been attributed to diffusional solvation. The solvation dynamics of DMSO consist of three components, with time scales of 214 fs, 2.3 ps, and 10.7 ps, and relative amplitudes of 50%, 41%, and 9%.[34] The fast component presumably corresponds to inertial solvation, whereas the slower, picosecond time scale components correspond to diffusional solvent relaxation.

Many examples have been reported in which the rate of intramolecular electron transfer is limited by the rate of inertial solvation.[28−30,36−38] The measured values of k_{ET} for Ru(II)−Pt(IV)−Ru(II) with $\chi_{DMSO} \leq 0.1$ are slower than the inertial solvation rates of water (2×10^{13} s^{-1}) and DMSO (4.7×10^{12} s^{-1}).[30,33,34] Thus, it is unlikely that inertial solvation dynamics are rate-limiting in the electron-transfer decay of Ru(III)−Pt(III)−Ru(II). On the other hand, the measured value of k_{ET} for aqueous Ru(II)−Pt(IV)−Ru(II) is significantly faster than the diffusional solvation rate of water (1.1×10^{12} s^{-1}), suggesting that the relaxation dynamics following MMCT are not governed by diffusional solvation. The ET dynamics of Ru(II)−Pt(IV)−Ru(II) slow with increasing χ_{DMSO}. However, the value of k_{ET} in the water/DMSO solvent mixtures is 2−10 times faster than the diffusional solvation rate of DMSO. Two other factors suggest that the decrease of k_{ET} in the water/DMSO mixed solvents is inconsistent with diffusion-controlled ET dynamics: diffusional solvation accounts for less than half of the overall solvent response, and water comprises the vast majority of the solvent for all solvent systems studied. On the basis of the above arguments, we conclude that neither inertial nor diffusional solvation controls the electron-transfer dynamics.

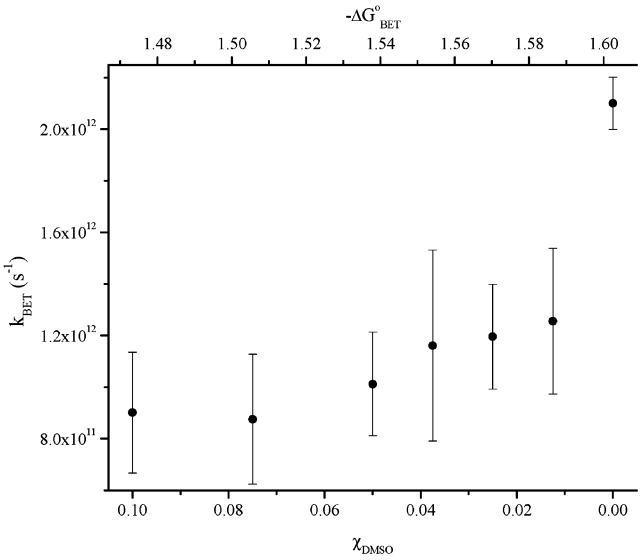

Figure 6. Plot of k_{BET} vs χ_{DMSO} and $-\Delta G°_{BET}$ for one-color pump−probe data of Ru(II)−Pt(IV)−Ru(II).

Instead, we focus on the effect that solvent-induced shifting of the Ru(II)−Pt(IV)−Ru(II) potential energy surface exerts on k_{ET}. Separation of k_{ET} into k_{BET} and k_{FET} is possible using the following relationship between k_{FET}, k_{ET}, and ϕ, the photodissociation quantum yield of Ru(II)−Pt(IV)−Ru(II).

$$\phi = \frac{k_{FET}}{k_{BET} + k_{FET}} = \frac{k_{FET}}{k_{ET}} \qquad (3)$$

Using the measured k_{ET} value of $2.10 \times 10^{12} \pm 1.0 \times 10^{11}$ s^{-1} and ϕ value of 0.001 for Ru(II)−Pt(IV)−Ru(II) in water,[11] k_{FET} is calculated to be $2.10 \times 10^{10} \pm 1.0 \times 10^{9}$ s^{-1}. Therefore, k_{BET} is approximately equal to k_{ET}. As previously discussed, the linear dependence of ground-state MMCT energy on χ_{DMSO} indicates that the Ru(II)−Pt(IV)−Ru(II) potential energy surface shifts linearly with χ_{DMSO}. The exponential dependence of ϕ on χ_{DMSO} suggests that the Ru(III)−Pt(III)−Ru(II) and Ru(III)/Pt(II)/Ru(III) potential energy surfaces are solvent independent.[15] The activation barrier for FET, and therefore k_{FET}, should also be solvent independent. Thus for all solvent compositions tested, $k_{FET} \ll k_{BET} \sim k_{ET}$, and the measured dependence of k_{ET} on χ_{DMSO} is a result of solvent-dependent k_{BET}. A plot of k_{BET} vs χ_{DMSO} is shown in Figure 6 for Ru(II)−Pt(IV)−Ru(II) with $\chi_{DMSO} \leq 0.1$. The ground-state absorption bandwidth of Ru(II)−Pt(IV)−Ru(II) does not change with χ_{DMSO}, indicating that the MMCT reorganization energy is solvent independent from $0 < \chi_{DMSO} < 0.275$. Therefore, the observed linear dependence of Ru(II) → Pt(IV) MMCT energy on χ_{DMSO} (Figure 1) necessarily implies a linear dependence of $|\Delta G°_{BET}|$, the driving force for back electron transfer, on χ_{DMSO}. $|\Delta G°_{BET}|$ can be calculated as a function of χ_{DMSO}, on the basis of the previously reported total reorganization energy of MMCT in aqueous solution[9] and the measured dependence of the MMCT energy on χ_{DMSO}. As shown in Figure 6, k_{BET} decreases with decreasing $|\Delta G°_{BET}|$, corresponding to Marcus normal region behavior.[32,39] Normal region BET behavior implies non-nested ground- and excited-state potential energy surfaces, which is consistent with the high MMCT energies, large absorption bandwidths, and large reorganization energies of Ru(II)−Pt(IV)−Ru(II) and Fe(II)−Pt(IV)−Fe(II).[9,40]

Further evidence for normal region BET behavior is provided by the two-color pump−probe data for Ru(II)−Pt(IV)−Ru(II) and the one-color data for Ru(II)−Pt(IV)−Ru(II) with χ_{DMSO}

> 0.1 (Table 1). In these data, k_{obs} corresponds to a convolution of electron-transfer dynamics and ground-state vibrational relaxation dynamics. Intramolecular vibrational dynamics should not vary significantly with minor changes in the solvation sphere. Therefore, the observed steady decrease of k_{obs} with increasing χ_{DMSO} for the Ru(II)−Pt(IV)−Ru(II) mixed-solvent data must reflect changes in BET dynamics. As $|\Delta G°_{BET}|$ decreases with increasing χ_{DMSO}, k_{BET} decreases, corresponding to normal region behavior. Similarly, we attribute the large decrease of k_{obs} for aqueous Fe(II)−Pt(IV)−Fe(II) relative to aqueous Ru(II)−Pt(IV)−Ru(II) to the decrease in $|\Delta G°_{BET}|$ for Fe(II) relative to Ru(II).

Conclusions

Relaxation dynamics following M(II) → Pt(IV) MMCT depend on solvent and the identity of the M(II) center. One-color pump−probe data for Ru(II)−Pt(IV)−Ru(II) in water/DMSO mixtures with $\chi_{DMSO} \leq 0.1$ allowed for deconvolution of BET and vibrational relaxation dynamics. BET time scales ranged from 476 ± 23 fs ($\chi_{DMSO} = 0$) to 1110 ± 288 fs ($\chi_{DMSO} = 0.1$). Ground-state vibrational relaxation time scales of 1.5 to 2.7 ps correspond well with previously reported values in mixed-valence complexes.[27,29,30,41,42] The measured BET rates are significantly slower than the rates of inertial solvation of water or DMSO. The solvent dependence of the BET rate has been ascribed to shifts of the ground-state electronic potential energy surface and the resulting changes in $|\Delta G°_{BET}|$. The rate of BET decreased with decreasing $|\Delta G°_{BET}|$, corresponding to Marcus normal region BET behavior. The solvent dependence of $|\Delta G°_{BET}|$ allows for systematic control over both the quantum yield of photodissociation and the dynamics of electron transfer, rendering the M(II)−Pt(IV)−M(II) complexes as highly useful model complexes for studying intramolecular electron-transfer processes.

Acknowledgment. This work was funded by the National Science Foundation under grant No. CHE-0079169 and the state of New Jersey, which provided funds for the CULA Laser Facility utilization. D.F.W. gratefully acknowledges a student fellowship provided by the International Precious Metals Institute.

References and Notes

(1) Meyer, T. J. *Acc. Chem. Res.* **1978**, *11*, 94−100.
(2) Creutz, C. *Prog. Inorg. Chem.* **1983**, *30*, 1−73.
(3) Vogler, A. *Coord. Chem. Rev.* **1985**, *64*, 159−173.
(4) Scandola, F.; Indelli, M. T.; Chiorboli, C.; Bignozzi, C. A. *Top. Curr. Chem.* **1990**, *158*, 73−149.
(5) Brunschwig, B. S.; Creutz, C.; Sutin, N. *Coord. Chem. Rev.* **1998**, *177*, 61−79.
(6) Meyer, T. J. *Chem. Rev.* **1998**, *98*, 1439−1477.
(7) Zhou, M.; Pfennig, B. W.; Steiger, J.; Van Engen, D.; Bocarsly, A. B. *Inorg. Chem.* **1990**, *29*, 2456−2460.
(8) Pfennig, B. W.; Bocarsly, A. B. *Coord. Chem. Rev.* **1991**, *111*, 91−96.
(9) Pfennig, B. W.; Bocarsly, A. B. *J. Phys. Chem.* **1992**, *96*, 226−233.
(10) Wu, Y.; Pfennig, B. W.; Sharp, S. L.; Ludwig, D. R.; Warren, C. J.; Vicenzi, E. P.; Bocarsly, A. B. *Coord. Chem. Rev.* **1997**, *159*, 245−255.
(11) Chang, C. Characterization of Photochemically Active Hexacyanometalate Coordination Polymers and Their Applications for Energy Conversion. Ph.D. Thesis, Princeton University, Princeton, NJ, 1999.
(12) Pfennig, B. W.; Lockard, J. V.; Cohen, J. L.; Watson, D. F.; Ho, D. M.; Bocarsly, A. B. *Inorg. Chem.* **1999**, *38*, 2941−2946.
(13) Hennessy, M. H.; Soos, Z. G.; Watson, D. F.; Bocarsly, A. B. *J. Phys. Chem. B* **2000**, *104*, 10909−10914.
(14) Watson, D. F.; Bocarsly, A. B. *Coord. Chem. Rev.* **2001**, *211*, 177−194.
(15) Wu, Y.; Cohran, C.; Bocarsly, A. B. *Inorg. Chim. Acta* **1994**, *226*, 251−258.
(16) Wilhelm, T.; Piel, J.; Riedle, E. *Opt. Lett.* **1997**, *22*, 1494−1496.
(17) Cerullo, G.; Nisoli, M.; De Silvestri, S. *Appl. Phys. Lett.* **1997**, *71*, 3616−3618.
(18) Shirakawa, A.; Kobayashi, T. *Appl. Phys. Lett.* **1998**, *72*, 147−149.
(19) Tan, H.-S.; Warren, W. S.; Schreiber, E. In *Ultrafast Phenomena XII*; Elsaesser, T., Mukamel, S., Murnane, M. M., Scherer, N. F., Eds.; Springer-Verlag: Berlin, 2001; p 105.
(20) Vardeny, Z.; Tauc, J. *Opt. Commun.* **1981**, *39*, 396−400.
(21) Eichler, H. J.; Langhans, D.; Massmann, F. *Opt. Commun.* **1984**, *50*, 117−122.
(22) Weiner, A. M.; Ippen, E. P. *Chem. Phys. Lett.* **1985**, *114*, 456−460.
(23) Palfrey, S. L.; Heinz, T. F. *J. Opt. Soc. Am. B: Opt. Phys.* **1985**, *2*, 674−679.
(24) Ekvall, K.; van der Meulen, P.; Dhollande, C.; Berg, L.-E.; Pommeret, S.; Naskrecki, R.; Mialocq, J.-C. *J. Appl. Phys.* **2000**, *87*, 2340−2352.
(25) Akesson, E.; Walker, G. C.; Barbara, P. F. *J. Chem. Phys.* **1991**, *95*, 4188−4194.
(26) Walker, G. C.; Akesson, E.; Johnson, A. E.; Levinger, N. E.; Barbara, P. F. *J. Phys. Chem.* **1992**, *96*, 3728−3736.
(27) Kliner, D. A. V.; Tominaga, K.; Walker, G. C.; Barbara, P. F. *J. Am. Chem. Soc.* **1992**, *114*, 8323−8325.
(28) Tominaga, K.; Kliner, D. A. V.; Johnson, A. E.; Levinger, N. E.; Barbara, P. F. *J. Chem. Phys.* **1993**, *98*, 1228−1243.
(29) Reid, P. J.; Silva, C.; Barbara, P. F.; Karki, L.; Hupp, J. T. *J. Phys. Chem.* **1995**, *99*, 2609−2616.
(30) Kambhampati, P.; Son, D. H.; Kee, T. W.; Barbara, P. F. *J. Phys. Chem. A* **2000**, *104*, 10637−10644.
(31) Son, D. H.; Kambhampati, P.; Kee, T. W.; Barbara, P. F. *J. Phys. Chem. A* **2002**, *106*, 4591−4597.
(32) Barbara, P. F.; Meyer, T. J.; Ratner, M. A. *J. Phys. Chem.* **1996**, *100*, 13148−13168.
(33) Jimenez, R.; Fleming, G. R.; Kumar, P. V.; Maroncelli, M. *Nature* **1994**, *369*, 471−473.
(34) Horng, M. L.; Gardecki, J. A.; Papazyan, A.; Maroncelli, M. *J. Phys. Chem.* **1995**, *99*, 17311−17337.
(35) Chen, P.; Meyer, T. J. *Chem. Rev.* **1998**, *98*, 1439−1477.
(36) Tominaga, K.; Walker, G. C.; Kang, T. J.; Barbara, P. F. *J. Phys. Chem.* **1991**, *95*, 10485−10492.
(37) Heitele, H. *Angew. Chem., Int. Ed. Engl.* **1993**, *32*, 359−377.
(38) Yoshihara, K.; Tominaga, K.; Nagasawa, Y. *Bull. Chem. Soc. Jpn.* **1995**, *68*, 696−712.
(39) Marcus, R. A. *Angew. Chem., Int. Ed. Engl.* **1993**, *32*, 1111−1121.
(40) Pfennig, B. W.; Wu, Y.; Kumble, R.; Spiro, T. G.; Bocarsly, A. B. *J. Phys. Chem.* **1996**, *100*, 5745−5750.
(41) Doorn, S. K.; Dyer, R. B.; Stoutland, P. O.; Woodruff, W. H. *J. Am. Chem. Soc.* **1993**, *115*, 6398−6405.
(42) Doorn, S. K.; Stoutland, P. O.; Dyer, R. B.; Woodruff, W. H. *J. Am. Chem. Soc.* **1992**, *114*, 3133−3134.